The Dynamic Allan Variance V: Recent Advances in Dynamic Stability Analysis

Lorenzo Galleani[1], *Senior Member, IEEE,* Patrizia Tavella[2], *Senior Member, IEEE*
[1]Politecnico di Torino, 10129 Torino, Italy, Email: galleani@polito.it
[2]INRIM, 10135 Torino, Italy, Email: tavella@inrim.it

***Abstract*—The dynamic Allan variance (DAVAR) measures the stability variations of precise clocks and oscillators. When an anomaly occurs, the DAVAR changes with time, its shape depending on the anomaly. In this work, we first discuss our current knowledge about the DAVAR, by focusing on the meaning of dynamic stability. Then, we extend our knowledge by obtaining additional properties of the DAVAR. Furthermore, we visually investigate the DAVAR for the main anomalies of precise clocks and oscillators. Finally, we review a variety of applications based on the DAVAR.**

TIPS: VII (e) - Category: *FREQUENCY CONTROL* - Subcategory: *Frequency measurement and statistics*.

I. Introduction

Time has been steadily strengthening its key role in technology since the birth of electrical and electronic devices. Recently, this process has seen a steep acceleration, and today a growing number of applications depend heavily on accurate and reliable time references. Global navigation satellite systems (GNSSs) are among the most successful applications. In a GNSS the user position is estimated from the time of flight of the signals travelling from the satellites to the receiver. An error in time implies therefore an error in position, and high quality precise clocks are hence essential elements onboard satellites and in ground stations of GNSSs. Certified time has become a fundamental constraint also for time stamping of bank and stock market transactions. Moreover, telecommunications and computer networks, as well as smart grids, need accurate synchronization to a common time reference to operate.

This abundance of applications of precise timing explains the amount of research carried out to develop better precise clocks, the true masters of time. The primary quantity to describe the quality of a precise clock is stability, whose standard measure is the Allan variance [1]-[4]. The Allan variance is a function of the observation interval. The smaller the Allan variance for a given observation interval, the better the stability.

Experimental evidences show that the stability of a precise clock varies with time due to several reasons, such as temperature, humidity, vibrations, breakdowns, ageing, gravitational effects, and irradiations. Such time-varying stability can be described by the dynamic Allan variance (DAVAR) [5]-[10]. The DAVAR is a function of time and the observation interval. When the clock follows the specifications, the DAVAR is stationary with time and varies with respect to the observation interval only. When an anomaly occurs, the clock deviates from the specifications and the DAVAR changes also with respect to time, its shape depending on the type of anomaly.

In this article we collect, integrate, and clarify what we have understood so far about dynamic stability, namely, about a stability that changes with time. We collect the main results on the DAVAR, including the most recent ones on the study of clock anomalies. We integrate these results by obtaining additional properties and results on the DAVAR, such as the equivalence between the DAVAR and the Allan variance for a clock whose physical parameters do not change with time, the continuous-time DAVAR in case of missing data, the DAVAR for a linear frequency drift, the theoretical discrete-time DAVAR for a series of common nonstationary behaviors of precise clocks including a slow frequency jump, a change of drift, and a change of noise type. We refer to such nonstationary behaviors as nonstationarities. We clarify the meaning of dynamic stability by discussing the DAVAR of the most interesting nonstationarities of precise clocks. We take a visual approach. Whenever possible, we discuss pictures rather than formulas. The final goal is to build a visual guide to dynamic stability analysis.

In addition to dynamic stability analysis, the structure of nonstationary random processes can be investigated by using time-frequency analysis [11]-[13], a body of techniques for the representation of time-varying spectra, or wavelets [14], [15], which instead provide a description in the time-scale domain. Detrended fluctuation analysis, a technique based on piecewise regression analysis, has also proven to be a useful tool [16].

The article is organized as follows. In Sect. II we introduce our notation for time and frequency, we define the Allan variance, and then the DAVAR along with its estimator, fast computational algorithm, and visualization modes. In Sect. III we give a visual tour of the DAVAR for the main nonstationarities of precise clocks. Finally, in Sect. IV we discuss the applications of the DAVAR to the field of precise timing and to other fields.

II. Time, Frequency, Stability, and Dynamic Stability

We introduce the key quantities to characterize time, frequency, stability, and dynamic stability. The readers familiar with precise timing can skip the introduction to the time and frequency concepts given in Sect. II-A.

A. Time and Frequency

An ideal oscillator generates a sinusoidal signal of the form [17]

$$u(t) = U_0 \sin(2\pi\nu_0 t), \tag{1}$$

where U_0 and ν_0 are the nominal oscillation amplitude and frequency, respectively. For a real-world oscillator, a more effective model is given by

$$u(t) = (U_0 + \epsilon(t)) \sin(2\pi\nu_0 t + \varphi(t)), \tag{2}$$

where $\epsilon(t)$ represents the amplitude fluctuations and $\varphi(t)$ takes into account the fluctuations on the phase. We neglect the amplitude fluctuations and obtain the approximate model

$$u(t) = U_0 \sin(2\pi\nu_0 t + \varphi(t)). \tag{3}$$

If we now define

$$h_0(t) = t, \tag{4}$$

$$h(t) = t + \frac{\varphi(t)}{2\pi\nu_0}, \tag{5}$$

as the ideal and real clock reading, respectively, then we can define the time deviation as

$$x(t) = h(t) - h_0(t). \tag{6}$$

The time deviation is hence the deviation of the clock reading from an ideal time reference. Substituting,

$$x(t) = \frac{\varphi(t)}{2\pi\nu_0}. \tag{7}$$

We now consider the instantaneous oscillation frequency of the approximated oscillator (3),

$$\nu(t) = \nu_0 + \frac{1}{2\pi}\frac{d\varphi(t)}{dt}. \tag{8}$$

We define the normalized frequency deviation as

$$y(t) = \frac{\nu(t) - \nu_0}{\nu_0}. \tag{9}$$

From (6), (8), and (9), we obtain the classic connection between the normalized frequency deviation and the time deviation

$$y(t) = \frac{dx(t)}{dt}. \tag{10}$$

Experimental measurements show that the time and frequency deviations are made by noise components and deterministic trends.

B. The Allan Variance

The Allan variance is defined as

$$\sigma_y^2(\tau) = \frac{1}{2}\left\langle (\bar{y}(t+\tau) - \bar{y}(t))^2 \right\rangle, \tag{11}$$

where the average frequency deviation $\bar{y}(t)$ is given by

$$\bar{y}(t) = \frac{1}{\tau}\int_{t-\tau}^{t} y(t')dt', \tag{12}$$

and $\langle\rangle$ denotes time averaging. The square root of the Allan variance is the Allan deviation $\sigma_y(\tau)$. By using (10) we instead have

$$\sigma_y^2(\tau) = \frac{1}{2\tau^2}\left\langle (x(t+\tau) - 2x(t) + x(t-\tau))^2 \right\rangle. \tag{13}$$

If we now define the increment

$$\Delta(t,\tau) = \bar{y}(t+\tau) - \bar{y}(t), \tag{14}$$

$$= \frac{x(t+\tau) - 2x(t) + x(t-\tau)}{\tau}, \tag{15}$$

then the equivalent definitions (11) and (13) can be written as

$$\sigma_y^2(\tau) = \frac{1}{2}\left\langle \Delta(t,\tau)^2 \right\rangle. \tag{16}$$

If the random process $\Delta(t,\tau)$ is ergodic we can evaluate the Allan variance as

$$\sigma_y^2(\tau) = \frac{1}{2}E[\Delta(t,\tau)^2], \tag{17}$$

where E is the expected value.

When we have N measurements $x[0], \ldots, x[N-1]$ of the time deviation, sampled at time τ_0 so that $x[n] = x(n\tau_0)$ and $\tau = k\tau_0$, we can estimate the Allan variance as

$$\sigma_y^2[k] = \frac{1}{2k^2\tau_0^2}\frac{1}{N-2k} \times \sum_{m=0}^{N-2k-1} (x[m+2k] - 2x[m+k] + x[m])^2, \tag{18}$$

for $k = 1, \ldots, N/2 - 1$, where N is assumed to be even.

C. The Dynamic Allan Variance

The DAVAR is defined as [5]

$$\sigma_y^2(t,\tau) = \frac{1}{2(T_w - 2\tau)} \times \int_{t-T_w/2+\tau}^{t+T_w/2-\tau} E[(\bar{y}(t'+\tau) - \bar{y}(t'))^2]dt', \tag{19}$$

where T_w is the length of the analysis window and $0 < \tau < T_w/2$. The square root of the DAVAR is the dynamic Allan deviation (DADEV) $\sigma_y(t,\tau)$. The DAVAR is therefore a sliding version of the Allan variance. From (10), the equivalent definition obtained from the time deviation is

$$\sigma_y^2(t,\tau) = \frac{1}{2\tau^2(T_w - 2\tau)} \times \int_{t-T_w/2+\tau}^{t+T_w/2-\tau} E[(x(t'+\tau) - 2x(t') + x(t'-\tau))^2]dt', \tag{20}$$

where $0 < \tau < T_w/2$. By substituting the increment (14), both definitions (19) and (20) can be rewritten as

$$\sigma_y^2(t,\tau) = \frac{1}{2(T_w - 2\tau)}\int_{t-T_w/2+\tau}^{t+T_w/2-\tau} E[\Delta(t',\tau)^2]dt'. \tag{21}$$

We note that, contrary to the Allan variance, for the DAVAR requiring the ergodicity of the increment $\Delta(t,\tau)$ is unnecessary, because the expected value $E[\Delta(t',\tau)^2]$ does not replace a time average performed over an infinite time interval, as in (16). The definition of the DAVAR aims instead at tracking

the variations in stability of the clock by integrating out $E[\Delta(t',\tau)^2]$ with respect to time on the finite sliding interval $t - T_w/2 + \tau < t' < t + T_w/2 - \tau$.

DAVAR estimator. An estimate of the DAVAR from experimental measurements can be obtained as [5]

$$\sigma_y^2[n,k] = \frac{1}{2k^2\tau_0^2}\frac{1}{N_w - 2k} \times \sum_{m=n-N_w/2}^{n+N_w/2-2k-1} (x[m+2k] - 2x[m+k] + x[m])^2, \tag{22}$$

where $k = 1, \ldots, N_w/2 - 1$ (assuming N_w to be even), $t = n\tau_0$ and $\tau = k\tau_0$ as in (18), and the discrete-time analysis window N_w satisfies $T_w = N_w\tau_0$.

Confidence analysis. The estimate of the DAVAR obtained with (22) shows the typical fluctuations due to the estimation process. The fluctuations are larger at high observation intervals because the number $N_w - 2k$ of triplets $x[m+2k]$, $x[m+k]$, $x[m]$ averaged in (22) decreases when the observation interval $\tau = k\tau_0$ increases. A detailed discussion on the confidence of the DAVAR estimator is given in [7], where confidence surfaces are also defined. We note that the total variance [18] and the ThêoH variance [19] could be used to improve the confidence of the DAVAR estimate when a limited number of measurements is available.

The case of missing data. Clock data series obtained from experimental measurements may suffer from missing data. We consider the case of time deviation measurements. The DAVAR for the case of missing data can be written as

$$\sigma_y^2(t,\tau) = \frac{1}{2\tau^2\mu(\mathrm{B}(t,\tau))} \times \int_{\mathrm{B}(t,\tau)} E[(x(t'+\tau) - 2x(t') + x(t'-\tau))^2]dt', \tag{23}$$

where $\mathrm{B}(t,\tau)$ is the set of time values t' in the interval $t - T_w/2 + \tau \le t' \le t + T_w/2 - \tau$ for which all of the triplets $x(t'-\tau)$, $x(t')$, $x(t'+\tau)$ are available for a given τ in $0 < \tau < T_w/2$, and $\mu(\mathrm{B}(t,\tau))$ is the measure of $\mathrm{B}(t,\tau)$. If none of the triplets are available in $t - T_w/2 + \tau \le t' \le t + T_w/2 - \tau$, then $\mathrm{B}(t,\tau)$ is the empty set, $\mu(\mathrm{B}(t,\tau)) = 0$, and the DAVAR is not defined for that particular time t and observation interval τ. Conversely, if all of the triplets are available, then $\mathrm{B}(t,\tau) = (t - T_w/2 + \tau, t + T_w/2 - \tau)$ and $\mu(\mathrm{B}(t,\tau)) = T_w - 2\tau$. In general, $0 \le \mu(\mathrm{B}(t,\tau)) \le T_w - 2\tau$. We note that a similar approach is used in [20] for the evaluation of the Allan variance in case of missing data.

The estimator for the case of missing time deviation data is defined straightforwardly from (23) as [9]

$$\sigma_y^2[n,k] = \frac{1}{2k^2\tau_0^2}\frac{1}{\#\mathrm{B}[n,k]} \times \sum_{\mathrm{B}[n,k]} (x[m+2k] - 2x[m+k] + x[m])^2, \tag{24}$$

where $\mathrm{B}[n,k]$ is the set of time values m in the interval $n - N_w/2 \le m \le n + N_w/2 - 2k - 1$ (assuming N_w to be even) for which all of the triplets $x[m]$, $x[m+k]$, $x[m+2k]$ are available for a given k in $1 \le k \le N_w/2 - 1$, and $\#\mathrm{B}[n,k]$ denotes the number of elements of $\mathrm{B}[n,k]$. In general, similarly to the continuous-time case, $0 \le \#\mathrm{B}[n,k] \le N_w - 2k$.

Equivalence between the Allan variance and the DAVAR. We define a time-invariant clock as a clock that follows the specifications and whose physical parameters, therefore, do not change with time. For this type of clock the DAVAR equals the Allan variance. This property is straightforwardly obtained by noting that, for a time-invariant clock, the increment $\Delta(t,\tau)$ is ergodic, and hence, from (17), it is

$$E[\Delta(t,\tau)^2] = 2\sigma_y^2(\tau). \tag{25}$$

Substituting in (21),

$$\sigma_y^2(t,\tau) = \sigma_y^2(\tau), \tag{26}$$

and hence, as expected, the DAVAR equals the Allan variance at any time instant. By using this property we immediately obtain the DAVAR for the common clock noise components. For instance, consider a white frequency noise (WFN) with normalized frequency deviation

$$y(t) = q\xi(t), \tag{27}$$

where $\xi(t)$ is a white Gaussian noise with zero mean and autocorrelation function

$$R_\xi(t_1,t_2) = E[\xi(t_1)\xi(t_2)] = q\delta(t_1 - t_2). \tag{28}$$

The Allan deviation for this noise component is

$$\sigma_y(\tau) = \sqrt{q}\tau^{-1/2}. \tag{29}$$

Since $\Delta(t,\tau)$ is ergodic for a WFN, from (26) the DADEV is straightforwardly obtained as

$$\sigma_y(t,\tau) = \sqrt{q}\tau^{-1/2}. \tag{30}$$

Visualization modes. The DAVAR $\sigma_y^2(t,\tau)$ is a real non-negative quantity function of t and τ, therefore its representation is a surface in a three-dimensional space. Consequently, a common way of representing the DAVAR is a mesh plot. As an example, in Fig. 1 we show the average frequency deviation, obtained for $\tau_0 = 300$ s, of a nonstationary WFN whose Allan deviation is $10^{-11}\tau^{-1/2}$ for $0 \le t < 3.6 \times 10^5$ s, $2 \times 10^{-11}\tau^{-1/2}$ for 3.6×10^5 s $\le t < 5.4 \times 10^5$ s, and again $10^{-11}\tau^{-1/2}$ for 5.4×10^5 s $\le t \le 9 \times 10^5$ s. Therefore, at $\tau = \tau_0$ the Allan deviation is $\sigma_y(\tau_0) \simeq 5.77 \times 10^{-13}$. In Fig. 2 we show the corresponding Allan deviation, which has the typical slope of a WFN and does not reveal the change of variance. Figure 3 shows instead the DADEV as a mesh plot, obtained for a window length $T_w = 90000$ s. The DADEV, displayed with a sampling time of 18000 s, clearly highlights the change of variance of the clock noise, and from its slope we can also estimate the Allan deviation in the three regions of the time series.

An effective way of combining the information of the frequency deviation, Allan deviation and DADEV is to display them as in Fig. 4. We refer to this representation as "gallery mode" because the average frequency deviation $\bar{y}(t)$ and the Allan deviation $\sigma_y(\tau)$ hang on the panels of the 3D plot like

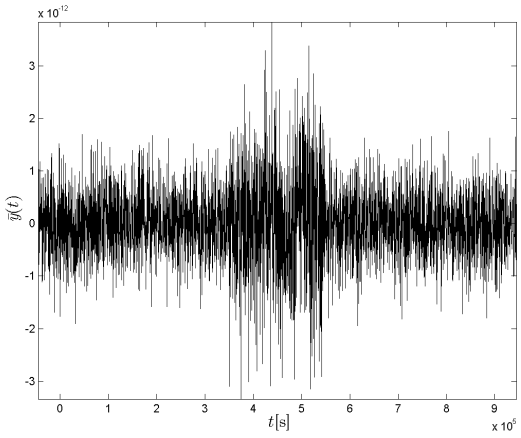

Fig. 1. Nonstationary WFN. The plot shows the average frequency deviation for $\tau_0 = 300$ s of a WFN whose Allan deviation $10^{-11}\ \tau^{-1/2}$ doubles in the region 3.6×10^5 s $\leq t \leq 5.4 \times 10^5$ s.

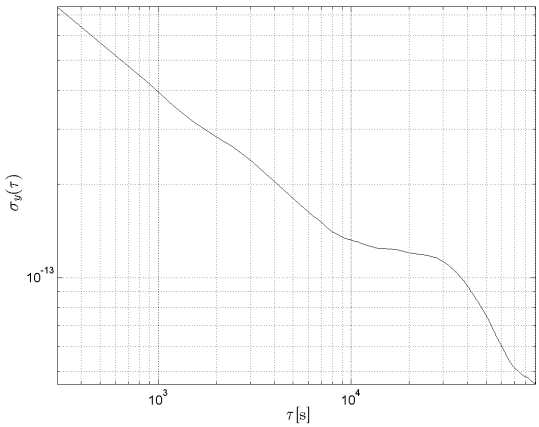

Fig. 2. Allan deviation of a nonstationary WFN. The plot shows the Allan deviation of the nonstationary WFN represented in Fig. 1. The slope of the Allan deviation indicates the presence of a WFN, but does not reveal the change of variance.

paintings in an art gallery. The primary advantage of this representation is the direct comparison between the DADEV and the frequency deviation, which better clarifies the nature of the observed nonstationarities. The gallery mode also displays the Allan deviation, which is the reference quantity for stability analysis.

A third possible way of displaying the DADEV is the waterfall plot shown in Fig. 5. This DADEV corresponds to a WFN whose variance increases suddenly at half the signal duration. The waterfall plot reveals this variation clearly. The advantage of the waterfall plot is that it allows to better observe the shape of the DADEV at different time instants. For a waterfall plot to be effective, though, the number of time instants at which the DADEV is computed must not be too large. In a time laboratory, the waterfall plot can be used to monitor the real-time evolution of the dynamic clock stability by displaying, for instance on a daily basis, a new stability curve computed also with the most recent available data, and by erasing the oldest curve.

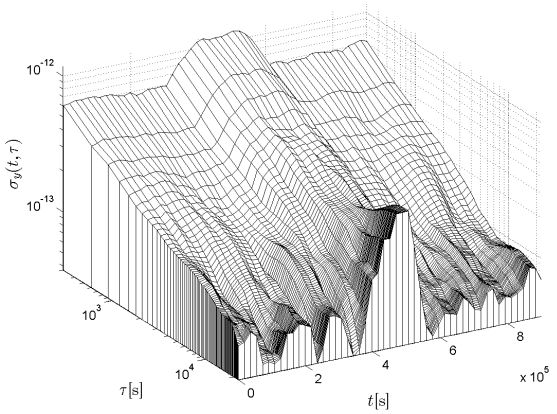

Fig. 3. DADEV of a nonstationary WFN. The plot shows the DADEV of the nonstationary WFN represented in Fig. 1. The DADEV clearly highlights the change of variance of the clock noise.

BeginExpansion
Computational algorithm. The DAVAR can be estimated from experimental measurements by using (22) when all the data are available, or by using (24) when some data are missing. The computational time required by a direct implementation of these estimators can be large for long time series. Fortunately, the fast algorithm [6] dramatically reduces the computational cost of the DAVAR. The fast algorithm is based on a recursive implementation of the DAVAR, which works also in the case of missing data.

Software implementations. The DAVAR has been implemented in the main software programs for the characterization of precise clocks and oscillators, including:

- Stable32: the commercial reference software for stability analysis [21].
- The GPS Toolkit (GPSTk): an open source software for the analysis of GPS data developed by the Space and Geophysics Laboratory of the Applied Research Laboratories, at The University of Texas at Austin. For a description of this software see [22].
- CANVAS (Clock Analysis, Visualization, and Archiving System): a software for clock analysis developed by the U.S. Naval Research Laboratory [23].

III. Understanding Dynamic Stability

The best way to understand the variations with time of the clock stability is to carefully analyze the DAVAR for the most common nonstationarities occurring in precise clocks and oscillators. We first consider the case of a clock following the specifications, and then we go through a series of the most common anomalies that occur to precise clocks, and particularly to space clocks. For all of the considered examples, we show the gallery mode of the DAVAR estimated from simulated data, and then the mesh plot of the theoretical DAVAR obtained either from analytical calculations, or estimated by averaging a large number of simulated realizations (Monte Carlo simulations). Such simulations can be performed

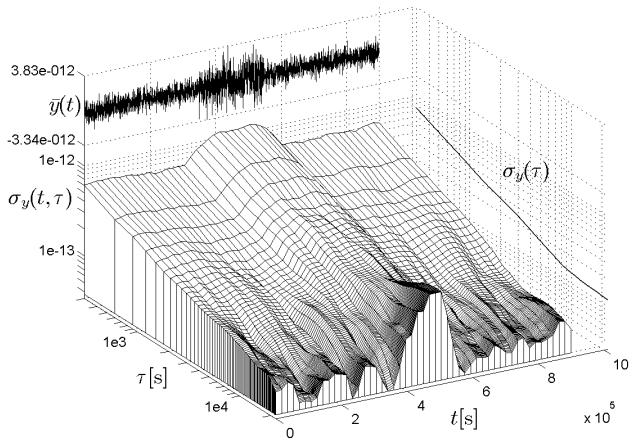

Fig. 4. Gallery mode representation of the DADEV of a nonstationary WFN. The top plot shows the average frequency deviation of the nonstationary WFN represented in Fig. 1. The side plot shows the corresponding Allan deviation represented in Fig. 2. The mesh plot shows the DADEV represented in Fig. 3.

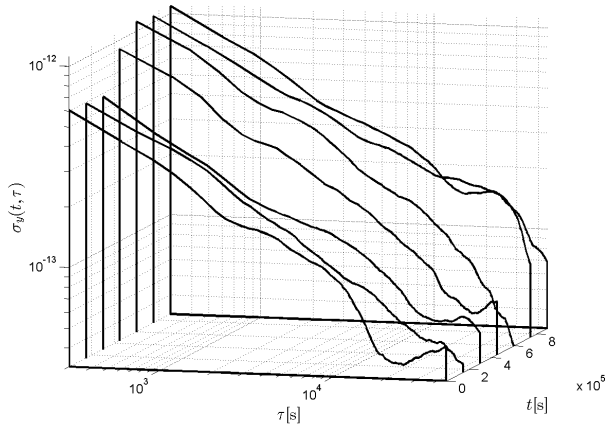

Fig. 5. Waterfall plot of the DADEV of a nonstationary WFN. The plot shows the waterfall representation of the DADEV of a WFN whose variance increases suddenly at half the signal duration. The waterfall plot simplifies the analysis of the DADEV at every time instant. The effectiveness of this plot is higher when the number of time instants is small.

with the clock models given in [24], [25]. The comparison of the estimated and the theoretical DAVAR better clarifies the meaning of dynamic stability analysis of precise clocks.

In all of the examples we consider a clock characterized by a WFN whose Allan deviation is

$$\sigma_y(\tau) = 10^{-11}\tau^{-1/2}. \tag{31}$$

We consider $T = 9 \times 10^5$ s of data sampled at $\tau_0 = 300$ s. Therefore, as in the example of Fig. 2, at $\tau = \tau_0$ the Allan deviation is $\sigma_y(\tau_0) \simeq 5.77 \times 10^{-13}$. These specifications correspond, for example, to a Rubidium clock for space applications. For all of the examples, the window length of the DAVAR is $T_w = 90000$ s. Moreover, all of the anomalies occur on time instants multiples of the sampling time τ_0.

A. Time-Invariant Clock

We first consider a time-invariant clock that follows the expectations (31). In Fig. 6 we show the gallery mode representation of the DAVAR. The top plot shows one realization of the average frequency deviation $\bar{y}(t)$ obtained for $\tau = \tau_0$. The side plot is the estimated Allan deviation obtained by using (18). The slope of the Allan deviation is $\tau^{-1/2}$, and it correctly indicates the presence of a WFN. The mesh plot is the DADEV estimated by using (22). Aside from the fluctuations due to the estimation process, the DADEV is apparently stationary with time, and its slope corresponds to a WFN.

Figure 7 shows instead the theoretical DADEV, which is a deterministic surface. We see that the theoretical DADEV is stationary with time, and its slope corresponds to the WFN given in the specifications (31). From (26) in fact, for a time-invariant clock the theoretical DADEV equals at any time instant the Allan deviation, and therefore the hypothesis of stationarity drawn from the DADEV in Fig. 6 is indeed correct. Therefore, the theoretical DADEV is instrumental in understanding the clock behavior, because its variations with time are caused solely by the nonstationarities occurring in the clock data.

B. Phase Jump

We consider a phase jump occurring at half the signal duration. The average frequency deviation in Fig. 8 shows the delta function corresponding to the phase jump, a consequence of the frequency deviation being the derivative of the time deviation, as described by (10). The Allan deviation in the side plot does not show this nonstationarity. Conversely, the DADEV reveals the presence of the phase jump, which locally deteriorates the clock stability. The absolute variation in the stability is larger at small observation intervals. The theoretical DADEV in Fig. 9 clearly shows the variation in stability due to the phase jump aside from the fluctuations due to the estimation process. We see that the variation in stability becomes more peaked as the observation interval increases. The DADEV corresponding to a phase jump is obtained analytically in [8], where the dependence on the DADEV window length is also given explicitly.

C. Frequency Jump

Frequency jumps are common anomalies in precise clocks, and especially in space clocks. The average frequency deviation in Fig. 10 shows a frequency jump occurring at half the signal duration. The corresponding Allan deviation shows a variation in the slope, which could be due to several causes, such as a random walk frequency noise (RWFN), or to a linear frequency drift. The mesh plot shows instead the estimated DADEV, which highlights the presence of a WFN and of the frequency jump. The variation in stability caused by the frequency jump increases with the observation interval, because, contrary to the phase jump, the frequency jump is a permanent change in the clock behavior. The theoretical DADEV of the frequency jump can be computed analytically [8], and we show it in Fig. 11.

D. Slow Frequency Jump

The average frequency deviation of Fig. 12 shows a slow frequency jump, namely, a change in the mean value of the frequency deviation which happens in a finite time interval. Conversely, the frequency jump considered in Sect. III-C happens suddenly. A slow frequency jump is equivalent to a temporary change of frequency drift. Similarly to the frequency jump, the Allan deviation exhibits a variation in its slope, although this behavior can be due to different causes. The DADEV clearly reveals the structure of the clock noise, that is, the WFN component and the variation in stability due to the slow frequency jump. This variation in stability is spread over the time interval over which the jump occurs, and the peak in stability is smeared out with respect to the case of the frequency jump. Figure 13 instead shows the theoretical DADEV of the slow frequency jump, obtained by Monte Carlo simulations.

E. Change of Drift

The average frequency deviation in Fig. 14 shows a change of drift at half the signal duration. The Allan deviation shows a corresponding increase for large observation intervals. This increase can be due, for instance, to a sudden or slow frequency jump, as shown in Sects. III-C-III-D. The DADEV reveals instead the nonstationarity, since the initial zero drift corresponds to the typical slope of the WFN component, and then the drift change generates a variation in the dynamic stability. In Fig. 15 we show the theoretical DADEV for the change of drift. The variation in dynamic stability is clearly visible in the second part of the time series, and it can be explained analytically by computing the DADEV for the linear frequency drift

$$y(t) = y_0 + d\,t. \tag{32}$$

Its average frequency deviation is

$$\bar{y}(t) = y_0 + d\,t - \frac{1}{2}d\,\tau. \tag{33}$$

Therefore, the increment $\Delta(t,\tau)$ is given by

$$\Delta(t,\tau) = d\,\tau. \tag{34}$$

Replacing this result in the definition (21) of the DAVAR gives

$$\sigma_y^2(t,\tau) = \frac{1}{2}d^2\tau^2, \tag{35}$$

which corresponds to the Allan variance in presence of stationary drift. Therefore, the DADEV of a linear frequency drift is

$$\sigma_y(t,\tau) = \frac{\sqrt{2}}{2}d\,\tau, \tag{36}$$

and it corresponds to the behavior observed in Figs. 14-15.

F. Sinusoidal Term

A sinusoidal term is commonly observed in space clock estimates, and it can be due, for instance, to a residual of the orbit, or to relativistic effects, or to periodic changes of the environmental parameters. The average frequency deviation in Fig. 16 shows the presence of a sinusoidal term added to the WFN component. The corresponding Allan deviation shows the typical bump. The estimated DADEV shows a bump along the τ axis, but also an oscillation in time. The DADEV of a sinusoidal term

$$y(t) = A\cos(2\pi f_0 t + \varphi) \tag{37}$$

can be in fact computed analytically [8], and it is given by

$$\sigma_y(t,\tau) = \sigma_y(\tau)\sqrt{1-\alpha(\tau)\cos(4\pi f_0 t + 2\varphi)}, \tag{38}$$

where $\sigma_y(\tau)$ represents here the Allan deviation of a sinusoid,

$$\sigma_y(\tau) = A\frac{\sin^2\pi f_0\tau}{\pi f_0\tau}, \tag{39}$$

and

$$\alpha(\tau) = \frac{\sin 4\pi f_0(\tau - T_w/2)}{4\pi f_0(\tau - T_w/2)}. \tag{40}$$

Therefore, the oscillation in time of the DADEV is due to the term $\cos(4\pi f_0 t + 2\varphi)$, whereas the behavior along the τ axis depends both on $\sigma_y(\tau)$ and $\alpha(\tau)$. The effect of a sinusoid on dynamic stability can be better observed in the theoretical DADEV shown in Fig. 17.

G. Change of Variance

A change of variance is shown in the average frequency deviation of Fig. 18. The Allan deviation averages out this nonstationarity, and it shows the typical curve for a WFN. The DADEV reveals instead this increase in variance, and by measuring the slope before and after this change we can characterize the clock noise. The DADEV for a change of variance can be obtained analytically [8]. By using this result, we can generate the theoretical DADEV in Fig. 19.

H. Change of Noise Type

Changes of noise type can be observed in experimental data. In Fig. 20 we show the average frequency deviation of a WFN which, at half the signal duration, becomes a white phase noise (WPN) with higher intensity. The Allan deviation averages out the two noise regions, and hence it does not clearly reveal the transition. The DADEV instead shows the WFN region first, and then the transition to the WPN region. By estimating the slopes in these two regions we can characterize the clock noise. In Fig. 21 we show the theoretical DADEV obtained by Monte Carlo simulations.

I. Missing Data

In Fig. 22 we show the average frequency deviation of a stationary WFN with two blocks of missing data. The estimated Allan deviation obtained with the method in [20] is shown in the side plot. The estimated DADEV obtained with (24) is shown in the mesh plot. The blocks of missing data are represented by "canyons" in the mesh plot [9]. Even with missing data we can analyze the local variations of the stability and characterize the clock. In Fig. 23 we show the theoretical DADEV obtained by Monte Carlo simulations.

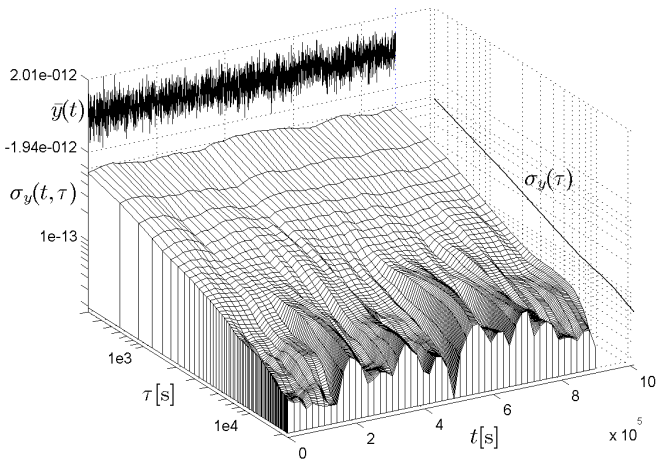

Fig. 6. White frequency noise. The top plot shows a WFN, and the side plot its Allan deviation. The DADEV (mesh plot) is stationary with time, aside from the fluctuations caused by the estimation process.

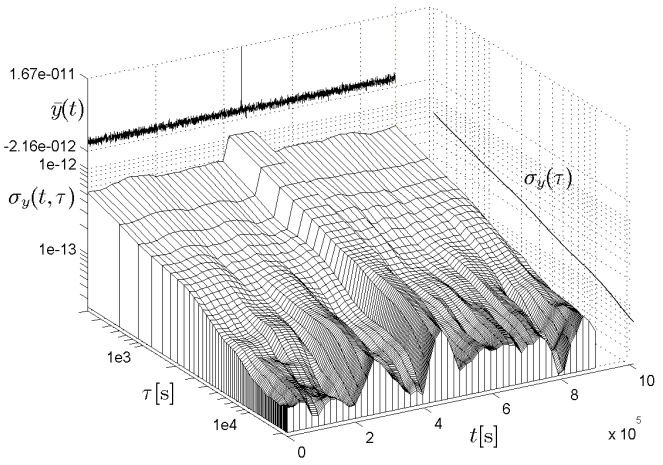

Fig. 8. WFN with a phase jump. The mesh plot shows the DADEV of a phase jump, whose average frequency deviation is a delta function (top plot). The Allan deviation (side plot) averages out the phase jump and does not reveal it.

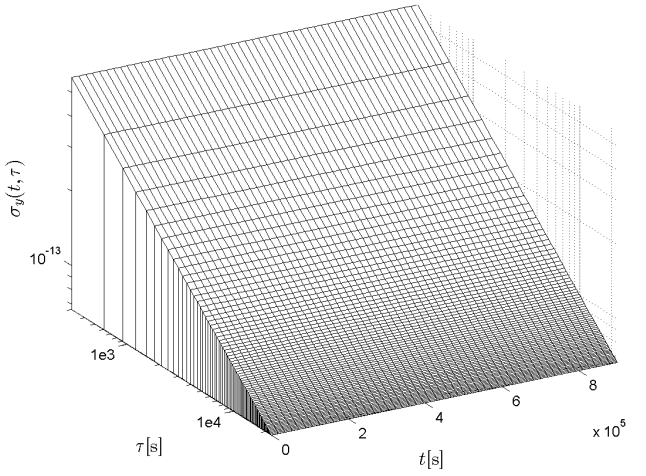

Fig. 7. Theoretical DADEV of a WFN. The plot shows the theoretical DADEV, obtained by analytical calculations, of the WFN in Fig. 6.

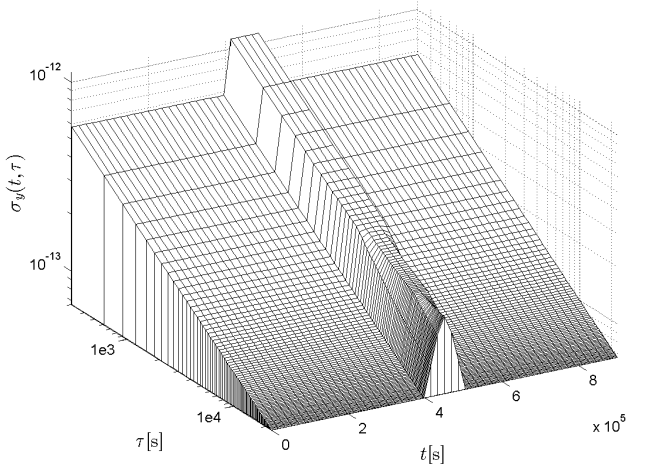

Fig. 9. Theoretical DADEV of a WFN with a phase jump. The plot shows the theoretical DADEV, obtained by analytical calculations, of the WFN with a phase jump in Fig. 8. The effect of the phase jump decreases at large τ values.

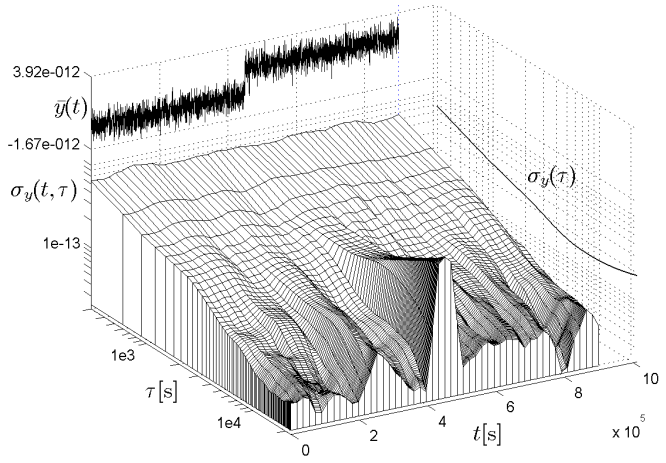

Fig. 10. WFN with a frequency jump. The top plot shows a WFN with a frequency jump, and the side plot its Allan deviation. The DADEV (mesh plot) clearly reveals the frequency jump.

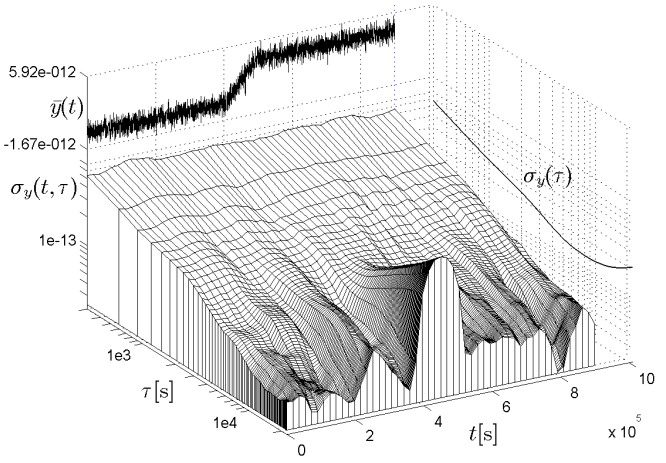

Fig. 12. WFN with a slow frequency jump. The top plot shows a WFN with a slow frequency jump, and the side plot its Allan deviation. The DADEV (mesh plot) reveals the slow frequency jump.

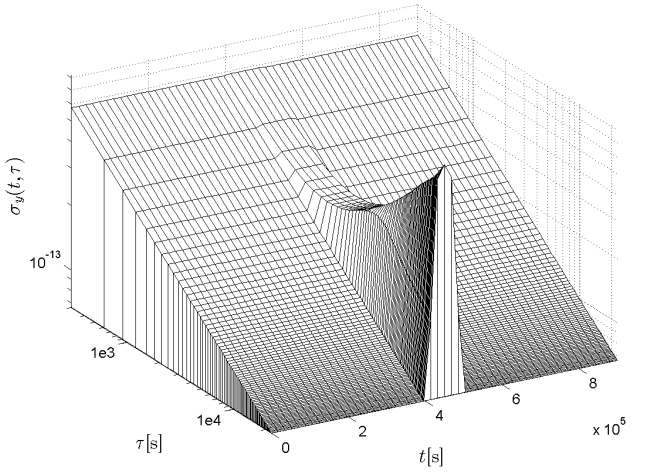

Fig. 11. Theoretical DADEV of a WFN with a frequency jump. The mesh plot shows the theoretical DADEV, obtained by analytical calculations, of the WFN with a frequency jump shown in Fig. 10. The dynamic stability of the frequency jump decreases with τ.

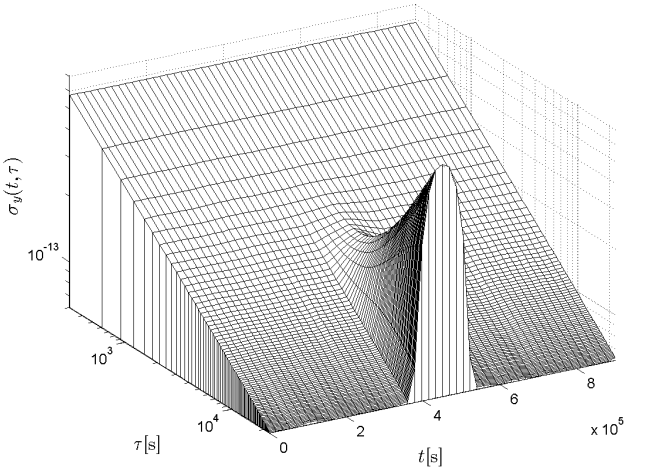

Fig. 13. Theoretical DADEV of a WFN with a slow frequency jump. The mesh plot shows the DADEV, obtained by Monte Carlo simulations, of the WFN with a slow frequency jump in Fig. 12. The dynamic stability of the slow frequency jump decreases with τ.

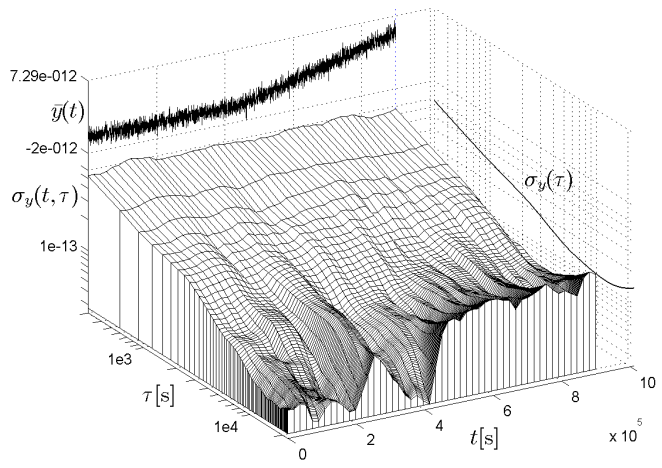

Fig. 14. Change of drift. The top plot shows a WFN whose drift changes. The side plot is the corresponding Allan deviation. The DADEV (mesh plot) shows a decrease in stability when the initial zero drift changes.

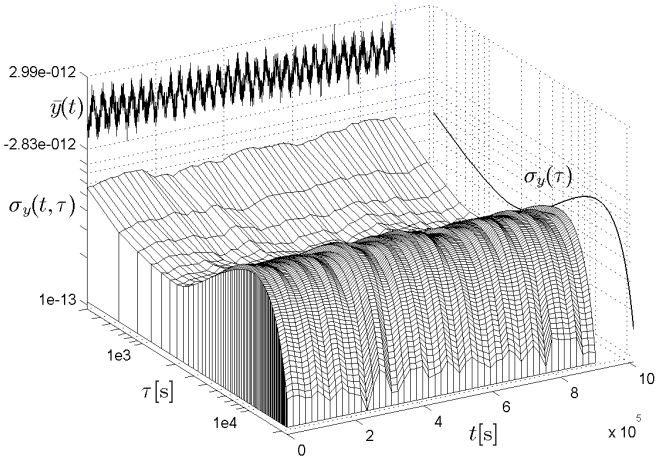

Fig. 16. Sinusoidal term. The top plot shows a WFN with a sinusoidal term, whereas the side plot shows its Allan deviation. The DADEV (mesh plot) shows that the sinusoid generates a bump along the τ axis, and an oscillatory behavior along the t axis.

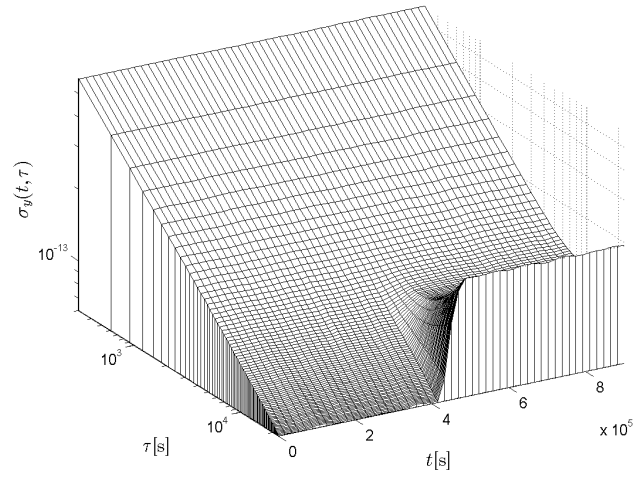

Fig. 15. Theoretical DADEV of a change of drift. The plot shows the theoretical DADEV, obtained by Monte Carlo simulations, of the change of drift in Fig. 14. The transition between the two drift regions is clear.

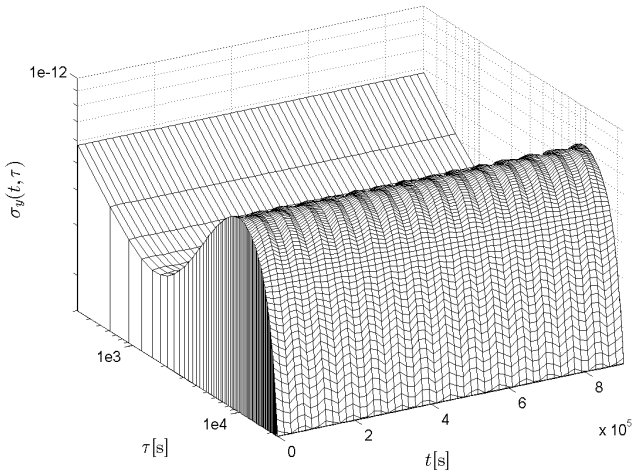

Fig. 17. Theoretical DADEV of a sinusoidal term. The plot shows the theoretical DADEV, obtained by analytical calculations, of the WFN with a sinusoidal term shown in Fig. 16. The oscillations in time are clearly visible.

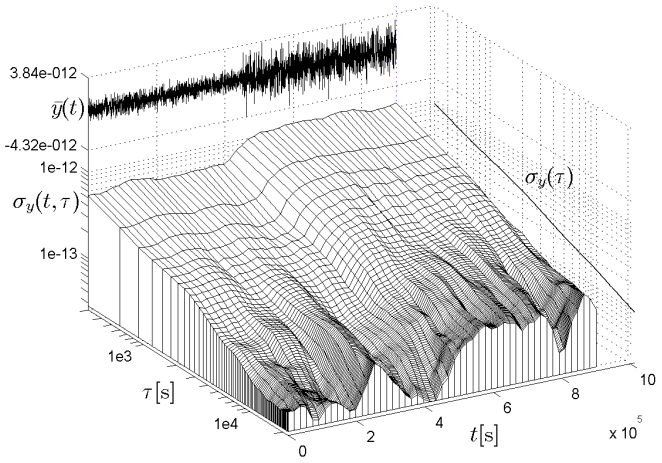

Fig. 18. Change of variance. The top plot shows a WFN whose variance changes suddenly. The DADEV (mesh plot) reveals the change of variance, which is averaged out by the Allan deviation (side plot).

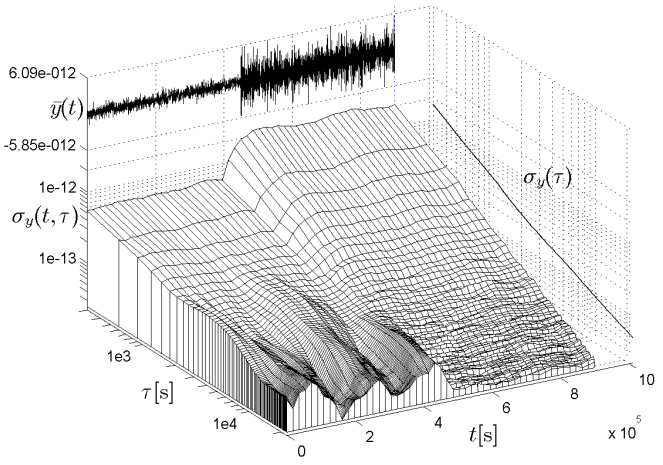

Fig. 20. Change of noise. The top plot shows a WFN which changes into a WPN. The Allan deviation (side plot) averages out the two noise regions, whereas the DADEV (mesh plot) clearly reveals them.

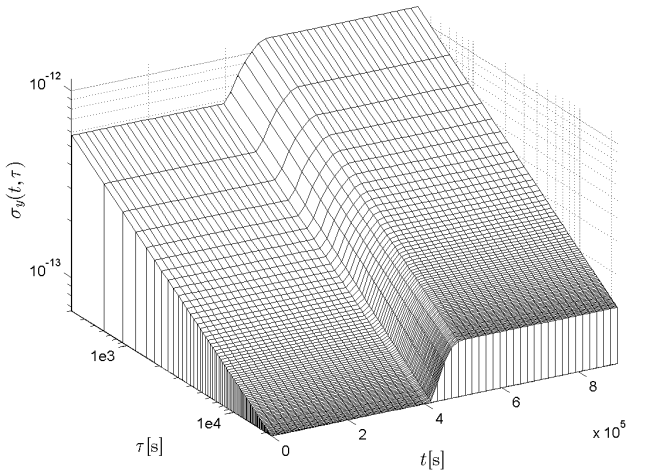

Fig. 19. Theoretical DADEV of a change of variance. The plot shows the DADEV, obtained by analytical calculations, of the WFN with a change of variance in Fig. 18. The transition between the two variance levels is clearly visible.

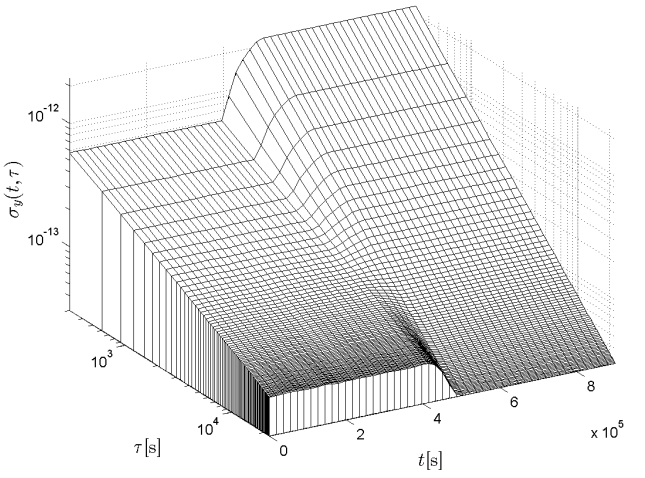

Fig. 21. Theoretical DADEV of a change of noise. The plot shows the theoretical DADEV, obtained by Monte Carlo simulations, of the WFN and WPN components in Fig. 20.

IV. Applications of the Dynamic Allan Variance

We discuss the application of the DAVAR to the field of precise timing and to other fields.

A. Applications to Precise Timing

The DAVAR is a tool specifically designed to characterize the stability of precise clocks and oscillators, therefore its primary field of application is precise timing. Consequently, we first discuss applications of the DAVAR to precise timing.

Clock characterization. The DAVAR can be used to characterize the behavior of a precise clock embedded in a complex system, for instance a space clock onboard a satellite of a GNSS. As a matter of fact, the DAVAR is routinely used by the U.S. Naval Research Laboratory to characterize the GPS clocks [26], [27]; it was used to characterize the Galileo clocks of the experimental satellites GIOVE-A and GIOVE-B [28]**;** it has been proposed as a tool to increase the robustness of the time references used in deep space missions [29].

Clock anomaly detection. The DAVAR can be used to detect when the stability of a precise clock does not meet the specifications. This detection is achieved by defining a proper detection surface [7]. When the DAVAR crosses the detection surface, an anomaly is detected. For example, in Fig. 24 we show the DADEV of a clock noise made by the sum of a WPN and a WFN. The variance of the WPN component increases with time, but this increase is not noticeable in the average frequency deviation because it is hidden in the dominant WFN component. Also the Allan deviation does not point out this nonstationarity. The DADEV does reveal this increase in the WPN variance, but to actually highlight it we need the detection surface, which clearly points out the nonstationarity of the WPN component at low observation interval values.

For this reason, a DAVAR detector was proposed within the Galileo system time (GST) algorithm prototype, to continuously check the precise clocks used to generate the reference time scale for the Galileo system. A DAVAR detector is also part of a multidetector that routinely controls the behavior of the precise clocks onboard the satellites of Galileo and other GNSSs [30], [31].

Clock validation. Another possible use of the DAVAR is to visually prove that the stability of a clock follows the specifications. This application is particularly interesting for clock manufacturers, who can prove that the stability performances of their clocks remain constant throughout time. In Fig. 25 we show an example of such use [32]. The picture shows the DADEV of a new space Rubidium atomic frequency standard, named Robust-RAFS, developed by Orolia Switzerland SA (SpectraTime). The DADEV demonstrates that the stability of the Robust-RAFS is stationary with time and follows the specifications during the entire performance test.

Other dynamic quantities. The analysis of how the stability of a precise clock changes with time can be extended to other definitions of stability, such as the Hadamard variance and the time deviation [33]. In Fig. 26 we show, for instance, the dynamic Hadamard variance (DHVAR) of an ultra-stable

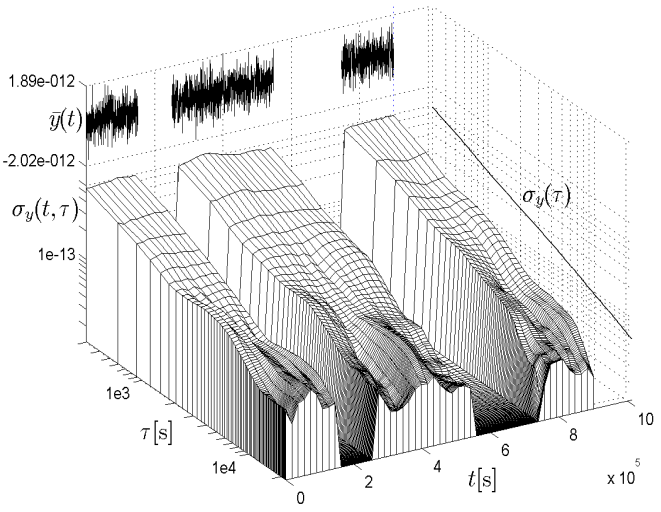

Fig. 22. Missing data. The top plot shows a stationary WFN with two blocks of missing data, and the side plot its Allan deviation. The DADEV reveals the WFN component in every region of available data, and it instead shows canyons where data are missing.

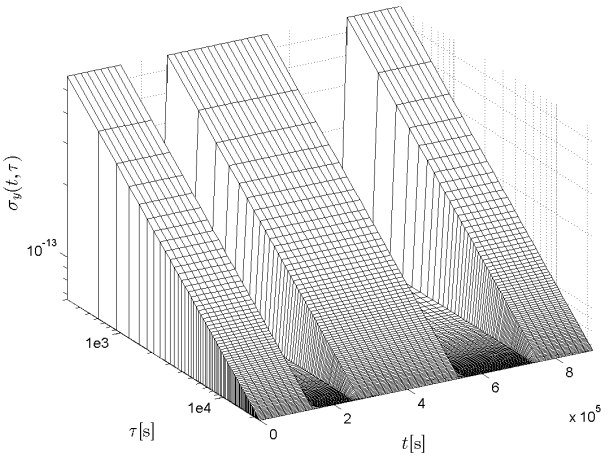

Fig. 23. Theoretical DADEV for missing data. The plot shows the DADEV, obtained by analytical calculations, of the WFN with missing data shown in Fig. 22.

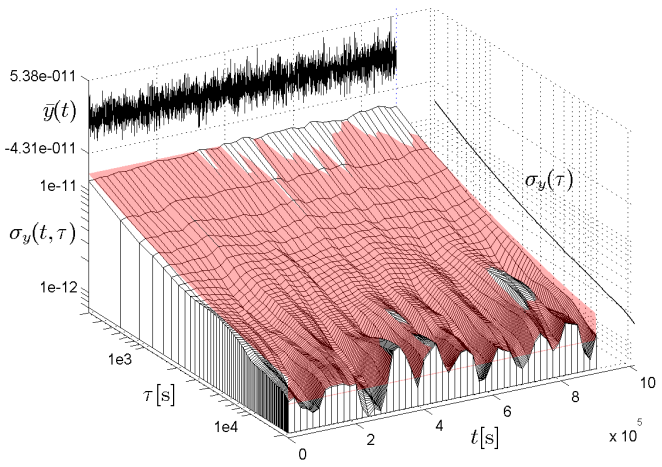

Fig. 24. Detection surface. The plot shows the DADEV of a clock noise made by the sum of a WPN component whose variance increases with time, and a WFN component. The detection surface highlights the nonstationarity of the WPN component, which is not noticeable in the average frequency deviation and in the Allan deviation.

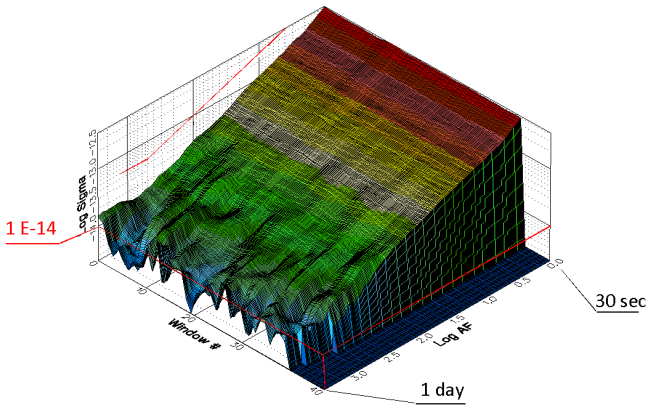

Fig. 25. Dynamic stability validation of a Rubidium clock. The mesh plot shows the DADEV of a new space Rubidium atomic frequency standard, the Robust-RAFS, developed by Orolia Switzerland SA (SpectraTime). By showing this picture, the clock manufacturer demonstrates to the customer that the Robust-RAFS follows the specifications throughout the entire performance test, and not just on the average, as it would prove with the Allan deviation only (side plot). (The picture is a courtesy of Fabien Droz [32].)

oscillator onboard the New Horizons deep space mission to the outer solar system [34]. The DHVAR indicates that the noise structure is probably made by a random walk flicker frequency noise, rather than a change of drift.

B. Other Applications

In addition to the noise of precise clocks and oscillators, the DAVAR can be used to investigate the structure of any non-stationary random process. Consequently, aside from precise timing, the DAVAR has been applied to other fields of science and engineering. An interesting application is the study of the heart interbeat rate [35]. In Fig. 27 we show the DADEV

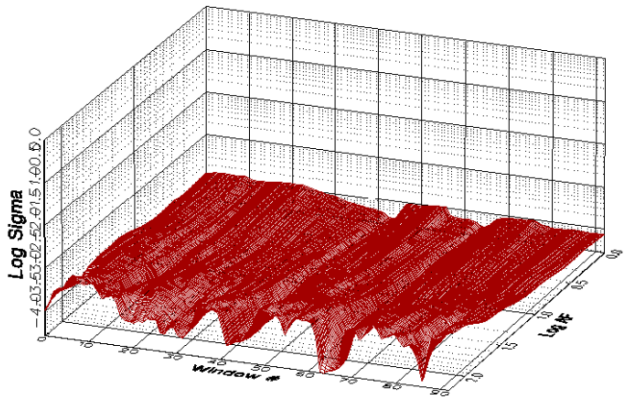

Fig. 26. Dynamic stability analysis of deep-space ultra-stable oscillators. The plot shows the dynamic Hadamard variance of an ultra-stable oscillator onboard the New Horizons space mission to the outer solar system. The DHVAR seems to imply the presence of a random walk flicker frequency noise in the oscillator data. (The picture is a courtesy of Gregory L. Weaver [34].)

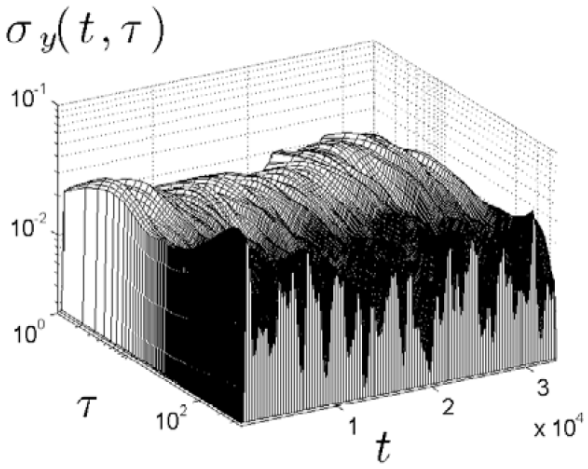

Fig. 27. DADEV of the heart interbeat rate for a normal patient. (The picture is a courtesy of Ricardo Hernández-Pérez [35].)

of the heart interbeat rate for a normal patient, whereas in Fig. 28 we show the DADEV of the heart interbeat rate for a patient suffering from congestive heart failure (CHF). The DADEV for the CHF case has a different shape and a richer nonstationary content. These differences in the DADEV structure can be used to better understand the mechanisms behind CHF and to classify physiological patients and patients suffering from CHF.

Among the other fields, the DAVAR has been also applied to characterize the noise of fiber optic gyroscopes (FOGs) [36], [37], and of sensors for robotic applications [38]. A DAVAR whose window length is adapted to FOG signals by using a fuzzy logic is proposed in [39].

V. Conclusions

We have presented what we have learned so far about the measure of dynamic stability. Our discussion focuses

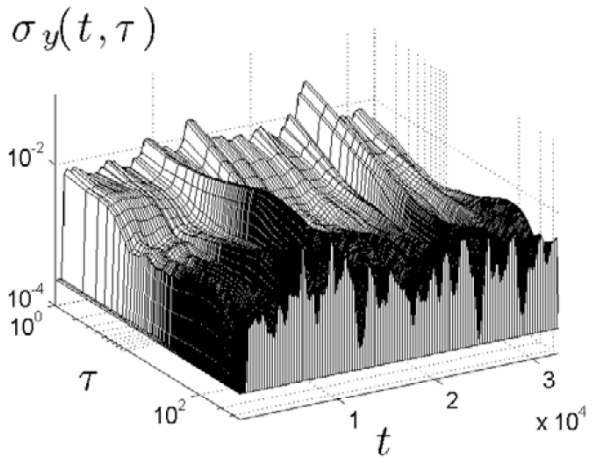

Fig. 28. DADEV of the heart interbeat rate for a patient suffering from CHF. The DADEV for this pathological patient shows a structure different from the DADEV of the physiological patient shown in Fig. 27. (The picture is a courtesy of Ricardo Hernández-Pérez [35].)

on the DAVAR, a measure of dynamic stability for precise clocks and oscillators. We have investigated the concept of dynamic stability by obtaining additional properties of the DAVAR and by visually representing it for the most common nonstationary behaviors of precise clocks and oscillators. We have also discussed some applications of the DAVAR to the field of precise timing and to other fields. The possibility to analytically evaluate the equations governing the DAVAR for the most common nonstationary behaviors, as well as its effective visual representation of anomalous behaviors, make the DAVAR an useful and sound tool for dynamic stability analysis, which can be applied not only to atomic clocks, but in general to any measured time series.

VI. Acknowledgements

We thank Fabien Droz from Orolia Switzerland SA (SpectraTime) for granting use of Figure 25, Gregory L. Weaver from the Applied Physics Laboratory at Johns Hopkins University for granting use of Fig. 26, and Ricardo Hernández-Pérez from Eutelsat Americas for granting use of Figs. 27-28.

References

[1] D. W. Allan, "Statistics of atomic frequency standards," *Proc. IEEE*, vol. 54, no. 2, pp. 221-230, 1966.

[2] D. W. Allan, "Time and Frequency (Time-Domain) Characterization, Estimation, and Prediction of Precision Clocks and Oscillators," *IEEE Trans. Ultra. Ferro. Freq. Contr.*, vol. 34, no. 6, pp. 647-654, 1987.

[3] IEEE Standard Definitions of Physical Quantities for Fundamental Frequency and Time Metrology, IEEE Std. 1139-1999.

[4] ITU-R Recommendation TF 538-3, "Measures for random instabilities in frequency and time (phase)," *International Telecommunication Union – Radiocommunication ITU-R*, vol. 2000, TF Series, Geneva, 2001.

[5] L. Galleani and P. Tavella, "The Dynamic Allan Variance," *IEEE Trans. Ultra. Ferro. Freq. Contr.*, vol. 56, no. 3, pp. 450-464, 2009.

[6] L. Galleani, "The Dynamic Allan Variance II: A Fast Computational Algorithm," *IEEE Trans. Ultra. Ferro. Freq. Contr.*, vol. 57, no. 1, pp. 182-188, 2010.

[7] L. Galleani, "The Dynamic Allan Variance III: Confidence and Detection Surfaces," *IEEE Trans. Ultra. Ferro. Freq. Contr.*, vol. 58, no. 8, pp. 1550-1558, 2011.

[8] L. Galleani and P. Tavella, "The Dynamic Allan Variance IV: Characterization of Atomic Clock Anomalies," *IEEE Trans. Ultra. Ferro. Freq. Contr.*, vol. 62, no. 5, pp. 791-801, May 2015.

[9] I. Sesia, L. Galleani, and P. Tavella, "Application of the Dynamic Allan Variance for the Characterization of Space Clock Behavior," *IEEE Trans. Aero. Elec. Sys.*, vol. 47, no. 2, pp. 884-895, Apr. 2011.

[10] L. Galleani and P. Tavella, "The Characterization of Clock Behavior with the Dynamic Allan Variance," *IEEE IFCS*, 5-8 May 2003, Tampa, FL.

[11] L. Cohen, *Time-Frequency Analysis*, Prentice-Hall, 1995.

[12] B. Boashash, *Time Frequency Analysis: A Comprehensive Reference*, Elsevier Science, 2003.

[13] L. Galleani, "Detection of changes in clock noise using the time-frequency spectrum," *Metrologia*, vol. 45, no. 6, pp. 143-153, Dec. 2008.

[14] M. Vetterli and J. Kovacevic, *Wavelets and Subband Coding*, CreateSpace Independent Publishing Platform, 2013.

[15] S. G. Mallat and G. Peyre, *A Wavelet Tour of Signal Processing: The Sparse Way*, Academic Press, 2008.

[16] J. W. Kantelhardta, S. A. Zschiegnera, E. Koscielny-Bundec, S. Havlind, A. Bundea, and H. E. Stanley, "Multifractal detrended fluctuation analysis of nonstationary time series," *Physica A*, vol. 316, no. 1–4, pp. 87–114, Dec. 2002.

[17] P. Kartaschoff, *Frequency and time*, Academic Press, 1978.

[18] C. A. Greenhall, D. A. Howe, and D. B. Percival, "Total Variance, an Estimator of Long-Term Frequency Stability," *IEEE Trans. Ultra. Ferro. Freq. Contr.*, vol. 46 , no. 5, Sept. 1999.

[19] D. A. Howe, "ThêoH: a hybrid, high-confidence statistic that improves on the Allan deviation," *Metrologia*, vol. 43, no. 4, pp. S322-S331, Aug. 2006.

[20] I. Sesia and P. Tavella, "The Allan variance for measurements with long periods of missing data and outliers," *Metrologia*, vol. 45, no. 6, pp. 134-142, Dec. 2008.

[21] Stable32 Software, Available at http://www.wriley.com/

[22] T. J. H. Craddock, R. J. Broderick, C. P. Petersen, and A. Hu, "The GPS Toolkit: Open Source Clock Tools," *40th Annual Precise Time and Time Interval (PTTI) Meeting*, 1-4 Dec. 2008, Reston, VA.

[23] K. Senior, R. Beard, and J. White, "CANVAS: clock analysis, visualization, and archiving system - a new software package for the efficient management of clock/oscillator data," *IEEE FCS 2005*, 29-31 Aug. 2005, Vancouver, BC.

[24] L. Galleani, "A tutorial on the two-state model of the atomic clock noise," *Metrologia*, vol. 45, no. 6, pp. 175-182, Dec. 2008.

[25] C. Zucca and P. Tavella, "A mathematical model for the atomic clock error in case of jumps," *Metrologia*, vol. 52, no. 4, pp. 514-521, Aug. 2015.

[26] R. Beard, Personal communication, May 2015.

[27] Naval Center for Space Technology, "Monthly analysis report – October 2006," U.S. Naval Research Laboratory, Washington DC, 2006.

[28] I. Sesia, L. Galleani, and P. Tavella, "Implementation of the Dynamic Allan Variance for the Galileo System Test Bed V2," *IEEE EFTF-FCS 2007*, 29 May - 1 Jun. 2007, Geneva, Switzerland.

[29] M. Miranian, G. L. Weaver, and M. J. Reinhart, "An ensemble of ultra-stable quartz oscillators to improve spacecraft on-board frequency stability," *38th Annual Precise Time and Time Interval (PTTI) Meeting*, 5–7 Dec. 2006, Reston, VA.

[30] A. Cernigliaro, G. Fantino, I. Sesia, L. Galleani, and P. Tavella, "Nonstationarities in space clocks: Investigations on Experimental Data," *28^{th} European Frequency and Time Forum (EFTF)*, 23-26 June 2014, Neuchâtel, Switzerland.

[31] I. Sesia, G. Signorile, G. Cerretto, E. Cantoni, P. Tavella, A. Cernigliaro, and A. Samperi, "Time metrology in the Galileo navigation system: The experience of the Italian National Metrology Institute," *2014 IEEE Metrology for Aerospace (MetroAeroSpace)*, 4-5 June 2015, Benevento, Italy.

[32] D. Fabien, R. Pascal, S. Boillat, and B. Scheidegger, "GNSS RAFS latest improvements," *presented at IFCS-EFTF 2015*, 12-16 April 2015, Denver, CO.

[33] A. Dobrogowski and M. Kasznia, "Real-time assessment of dynamic Allan deviation and dynamic time deviation," *2012 European Frequency and Time Forum (EFTF)*, 23-27 April 2012, Gothenburg.

[34] J. R. Jensen and G. L. Weaver, "Frequency Performance of the New Horizons Ultra-Stable Oscillators," *IEEE IFCS-EFTF 2015*, 12-16 April 2015, Denver, CO.

[35] R. Hernández-Pérez, L. Guzmán-Vargas, I. Reyes-Ramírez, and F. Angulo-Brown, "Evolution in time and scales of the stability of heart interbeat rate," *Europhysics Letters*, vol. 92, no. 6, Dec. 2010.

[36] C. Zhang, L. Wang, S. Gao, H. Li, T. Lin, X. Li, and T. Wang, "Dynamic Allan variance analysis for stochastic errors of fiber optic gyroscope," *Infrared and Laser Engineering*, vol. 43, no. 9, pp. 3081-3088, Sept. 2014.

[37] J. Li, F. Gao, G. Wang, W. Gao, W. Zhu, and M. Wang, "Analysis of dynamic Allan variance for fiber optic gyro under vibration and variable temperature conditions," *Chinese Journal of Lasers*, vol. 40, no. 9, Sept. 2013.

[38] S. Jain, S. Nandy, G. Chakraborty, C. S. Kumar, R. Ray, and S. N. Shome, "Error modeling of various sensors for robotics application using Allan variance technique," *2011 IEEE International Conference on Signal Processing, Communications and Computing (ICSPCC)*, 14-16 Sept. 2011, Xi'an.

[39] S. Gu, J. Liu, Q. Zeng, S. Feng, and P. Lv, "Dynamic Allan Variance Analysis Method with Time-Variant Window Length Based on Fuzzy Control," *Journal of Sensors*, vol. 2015, Article ID 564041, 8 pages, 2015.